Comparison of F_N One Speed Transport Solution in a Heterogeneous Slab to a Monte Carlo Energy Independent Solution

by

Robert C. Singleterry Jr.
Argonne National Laboratory - West
P.O. Box 2528
Idaho Falls, ID 83403-2528
and
Salim Jahshan
SNJ Consulting
3093 Homestead Lane
Idaho Falls, ID 83404

DISCLAIMER

Paper to be Submitted to the
American Nuclear Society 1996 Topic Meeting on Advances and Applications in Radiation Protection and Shielding
North Falmouth, MA, USA
April 21-25, 1996

Comparison of F_N One Speed Transport Solution in a Heterogeneous Slab to a Monte Carlo Energy Independent Solution

Robert C. Singleterry Jr.*
Argonne National Laboratory - West
P.O. Box 2528
Idaho Falls, ID 83403-2528
and
Salim Jahshan
SNJ Consulting
3093 Homestead Lane
Idaho Falls, ID 83404

Abstract

The F_N basis function expansion solution to the Boltzmann transport equation in Cartesian geometry is summarized and evaluated for several heterogeneous slabs of interest. The resultant scalar and angular fluxes and the critical slab thickness (when applicable) compare to the Monte Carlo transport evaluations by MCNP. A correspondence between the one-group macroscopic cross section used in the F_N code is made to energy independent synthetic MCNP microscopic cross sections. The F_N method produces comparable results to MCNP, requires fewer computer resources, but is limited to specific problem types.

I. INTRODUCTION

The demand for fast and accurate solutions to shielding and deep penetrating radiation problems is increasing for many kinds of technical applications. These extend from the traditional detailed shielding calculations required for nuclear power and research facilities to nuclear powered ships and spacecraft where protection of equipment and living organisms from external or on-board sources is required. Further, fast and accurate irradiation practices and activation rates are also in great demand for intricate applications such as medical radiation therapy where collateral damage is to be avoided. Any method used to solve these problems will always have some limitations. By considering the application's physical priorities, the computational method is chosen by comparing the efficiency of all the methods relevant to the application.

The F_N solution to the linear Boltzmann equations first suggested by Siewert, *et. al.*[1-6] has been developed and extended in a solution to the neutron component of the galactic cosmic ray cascade[7]. From this, a general multiple energy group, heterogeneous slab F_N solution with isotropic scattering has been created and compared successfully to an S_N solution[8].

Considered in this work is the one speed, homogeneous and heterogeneous slab problem. The F_N solution is compared to an equivalent Monte Carlo solution utilizing MCNP[9]. The MCNP solution employs energy independent absorption, scattering, and fission cross sections. While this new comparison adds to the confidence realized in the earlier comparison to the S_N method, it allows an initial investigation into evaluation and comparison of the

*Work supported by the U.S. Department of Energy, Reactor Systems, Development and Technology, under Contract W-31-109-Eng-38.

multiple speed solution to an energy dependent solution even though in this preliminary work the cross sections are one speed in the F_N method and energy independent in MCNP.

The F_N method is a basis function expansion solution to the Boltzmann transport equation for a heterogeneous slab. This analysis looks only at one speed, isotropic scattering, and multiple sectionally homogeneous adjacent sub-slabs for simplicity. The compared outputs consist of scalar and angular fluxes and the critical thickness when applicable.

II. Summary of the F_N Method Developed for Planar Geometry

For completeness, the F_N method is summarized here briefly. The one speed, one dimensional Boltzmann transport equation can be written as

$$\left[\mu\frac{\partial}{\partial x} + 1\right]\phi(x,\mu) = \frac{c_i}{2}\int_{-1}^{+1} d\mu'\phi(x,\mu') + \frac{1}{2}S(x),$$

with the boundary conditions

$$\phi(x_{i-1},\mu) = F_L^i(\mu) \quad \text{and} \quad \phi(x_i,-\mu) = F_R^i(\mu) \quad \text{for} \quad \mu > 0,$$

where, c_i is the scattering to total cross section ratio for slab i, x_{i-1} and x_i are the left and right boundaries of slab i, $S(x)$ is the distributed volumetric source, $F_L^i(\mu)$ is a known general function in the positive half range of μ at x_{i-1}, and $F_R^i(\mu)$ is a known general function in the negative half range of μ at x_i.

The Boltzmann equation can be transformed into a pair of Fredholm type singular integral equations by extending the angular variable, μ, into the upper and lower complex planes. The resultant equations are integrated over x and the complex variable. The singularities are treated with the Plemelj relations as described in Muskhelishvili[10]. Then, the flux values are expanded as

$$\phi(x_{i-1},-\mu) = F_L^i(\mu)e^{-\frac{x_i-x_{i-1}}{\mu}} + \frac{c_i}{2}\sum_{\alpha=0}^{N-1} a_\alpha^i\psi_\alpha(\mu), \tag{1a}$$

and

$$\phi(x_i,\mu) = F_R^i(\mu)e^{-\frac{x_i-x_{i-1}}{\mu}} + \frac{c_i}{2}\sum_{\alpha=0}^{N-1} b_\alpha^i\psi_\alpha(\mu), \tag{1b}$$

where $\psi_\alpha(\mu)$ are the basis functions and a_α^i and b_α^i are the expansion coefficients. The expansion coefficients are determined by a collocation scheme and matrix inversion. A post processing step is included to account for regularizing the singular integrals and to account for an instability in equations (1) when μ is small and α is large. The same manipulations are performed to obtained a set of equations for the interior slab points except that one of the boundary points is defined as the interior point.

III. Description of the MCNP Synthetic Cross Sections

Considered for this application is neutron transport in the energy range from 0 to 20 MeV. MCNP input requires microscopic cross sections, continuous in energy, to describing a two-body interaction with the events outcome consistent with real (e.g., quantum mechanical) reactions. Thus, three synthetic energy independent microscopic cross sections are developed for these comparisons consistent with MCNP input requirements. MCNP tracks the particle history as it traverses the problem geometry and interacts with its nuclei. The cross section sets control the interactions and stops the history when the energy falls below 10^{-11} MeV. The pure elastic potential scattering and the pure capture cross sections were developed earlier[11, 12], and an energy independent fission cross section with an all-prompt neutron yield of $\nu = 3.0$ and a fission neutron energy spectrum of 20.0 to 19.999 MeV is

developed for this work. The values of the macroscopic, one-speed cross section in the F_N evaluations are related to these microscopic cross sections of type x, which are constant in energy without being spectrum weighted, i.e.,

$$\Sigma_x^{FN} = \sum_i \frac{\int dE\phi(E)N_i\sigma_x^i(E)}{\int dE\phi(E)} = \sum_i N_i\sigma_x^i; \quad (2)$$

since $\sigma_x^i(E) = \sigma_x^i$. Further, since there is only one group, there are no inter-group transfer terms needed in the F_N formulation.

IV. Description of the Models Analyzed

To compare and evaluate MCNP and the F_N methods, three test case models are defined. The first is a ten mean free path thick homogeneous slab with a mono-directional beam impinging on the left face. The second model is the same slab with a distributed, isotropic source in the interior. Both of these sources are also used with a heterogeneous slab that is nine mean free paths thick. The third model is a critical homogeneous slab with a uniformly distributed fission source. The resultant scalar and angular flux values are compared along with the critical slab width when applicable.

The slab characteristics for the first two models consist of a homogeneous slab that is ten mean free paths thick and the material identified by the value of c. Three cases are modeled for c values equal to 0.1, 0.5, and 0.9. A heterogeneous slab, nine mean free paths thick, is divided into three equal sub-slabs with an increasing or decreasing set of c values.

MCNP evaluates a k_{eff} for a specific geometry and material configuration. Thus for the slab geometry, the critical slab width is obtained from Table 2.6 in Bell and Glasstone[13] for c values of 1.02, 1.05, 1.1, 1.2, 1.4, and 1.6. These slab thicknesses and material configurations are entered into the MCNP model and the corresponding eigenvalues calculated. If k_{eff} bounds 1.0 within the level of confidence determined, then this configuration is defined as the critical width.

To correspond to the one dimensional F_N solution of the transport equation, the MCNP model represents a rectangular slab with two opposite faces corresponding to the end points of the F_N solution, and the two sets of remaining parallel surfaces as reflected. Since MCNP reports all tallies per source neutron, the source definition in MCNP must weight each source neutron by the area or the volume of the source in order to correspond to the results reported by the F_N method. For the critical slabs, the F_N method normalizes its flux to the exiting flux as determined by MCNP[7].

For the first model, the source is described in the F_N method by a boundary condition. In MCNP, an extra region to the extreme left of the model is created where the mono-directional source is placed. For the second model, the distributed source is implemented as a volumetric source. For the MCNP critical slab model, the standard KCODE and KSRC definitions are implemented. For the F_N method, the critically condition of the transport operator is used

$$\left| \left[\mu \frac{\partial}{\partial x} + 1 \right] \phi(\Delta, \mu) - \frac{c}{2} \int_{-1}^{+1} d\mu' \phi(\Delta, \mu') \right| = 0,$$

where Δ represents the critical width and is the value searched for in the above condition.

The basic result from the F_N method is the angular flux. These are integrated through the collocation coefficients and the basis functions to create a scalar flux. The uncollided scalar flux is included to compare to the MCNP results. In MCNP, the scalar flux is given by the F2 tally. The angular flux is obtain from the F1 tally by

$$\psi(x, \mu_i) = \frac{F1}{2\pi A|\mu_i|w_i}, \quad (3)$$

where, A is the tally area, μ_i and w_i are the gauss-legendre abscissas and weights based on the cosine bins used to

gather the $F1$ tallies, and the $F1$ tally represents

$$F1 = \int_A \int_\mu \int_t \int_E J(\vec{r}, E, t, \mu)\, \mathrm{d}E\, \mathrm{d}t\, \mathrm{d}\mu\, \mathrm{d}A,$$

where the scalar current[9] is related to the flux by

$$J(\vec{r}, E, t, \mu) = |\mu|\, \Phi(\vec{r}, E, t)\, A.$$

For the MCNP runs, the default values of the physics and biasing parameters are used. This includes the use of implicit capture variance reduction. The parameters used in the F_N method do not affect the final results, just whether the code converges to the answer (angular flux), the precision of that answer, and the number of terms needed in the basis expansion, i.e. computer resources needed. In this respect, a point-wise angular flux tolerance of 10^{-5} was chosen for all F_N models.

V. Comparison of Computed Results

This analysis was performed on a VAX 4000-60 running VMS 5.5. Table 1 shows the relative computer times used to execute each model and some important parameters that drive the timing. Figures 1 and 2 show the F_N and MCNP homogeneous slab scalar flux results for the beam source and the distributed source. Figures 3 and 4 show the heterogeneous slabs scalar flux comparisons. Figures 5 through 10 show the scalar flux comparisons for the six critical slabs.

Figures 11 and 12 show the angular flux comparisons at the edges and center of the homogeneous slab for the beam and distributed sources with a c value of 0.9. Figures 13 and 14 show the same angular flux comparisons for some of the heterogeneous slab cases. Figure 13 shows the angular flux comparison for the beam source with decreasing c values from the left face. Figure 14 shows the angular flux comparison for the distributed source with increasing c values.

These comparisons are in very good agreement; however, a few discrepancies must be explained along with known behavior that must be exhibited by the F_N method in order to be validated against MCNP. The first discrepancy is from the beam source used by the F_N method. It was implemented as a delta function boundary flux condition over position and angle. The MCNP model used an extra region with a volumetric beam source to approximate the delta function over position. All source histories were then started in the same direction as the F_N source to approximate the delta function over angle. This causes MCNP to try and model an infinite source at a point. The angular flux values from MCNP at the $x = 0$ and $\mu = 1$, when plotted in Figures 11 and 13, cannot represent this effect correctly and therefore do not compare directly.

The MCNP method is a statistical simulation of the input model. The resultant tally estimated errors should degrade the further away the tally is from the source in phase space. This is clearly shown for the mono-directional beam source in all slab combinations (see Figure 1, 11, or 13). The deeper the tally surface is in the slab or the further away the angle bin is from 1.0, the larger the flux error band. This is due to the number of particles (or the weight of the particles for implicit capture variance reduction) that traverse the slab and interact with the tally surface and the resultant statistical manipulations that follow.

The distributed source results show a symmetry about the centerline of the slab (see Figures 2 and 12). For the heterogeneous results, a symmetry is shown in the scalar flux results between the slab with increasing c values and the slab with decreasing values since the slab and source combinations are just mirror images (see Figure 4). Because all points of the slab are the same *distance* away from the source, the statistical anomalies as seen in the mono-directional source are not present.

The angular flux results do not compare well at all positions. This is due to an added error that is not a function of the Monte Carlo method. In equation (3), μ_i should be the mean value, but only the average μ is

known for the bin. Therefore, if the flux gradient is large, the difference between the average and mean is large and thus the calculated angular flux is not correct. MCNP at present does not have an angular flux tally and our present method of estimating it from the F1 tally yields inaccurate results in these situations.

Table 2 shows the results from the critical slab models. The critical widths input into MCNP determine a k_{eff} that bounds 1.0 within about two standard deviations (confidence level of 95%) for all values of c except 1.05. Various situations were modeled to explain this discrepancy, but a reasonable explanation has not been found. However, the flux comparisons for all cases are symmetric about the slab center and are in good agreement even for a c of 1.05. Since the fission source is distributed through-out the slab, the beam source model statistical problem does not arise for the same reason used in the distributed source model.

VI. Conclusion

The F_N method calculates results very comparable to MCNP as shown in this paper. All discrepancies can be explained except for the k_{eff} value determined by MCNP for a c of 1.05. The F_N method as shown has a CPU utilization advantage when compared to MCNP; however, the F_N method at this time is limited to planar geometry. MCNP may take longer to generate results, but its ability to model a multitude of geometric configurations allows more problems to be modeled and answers obtained.

The comparison between a deterministic evaluation, such as the F_N method, and MCNP is possible because the one group macroscopic cross section can be easily related to the continuous energy microscopic cross sections (see Equation 2). When a deterministic code employs multiple group cross sections, the two sets of deterministic multiple group cross section and synthetic MCNP cross sections will have to be shown to correspond before code comparisons can be made.

Acknowledgments

We would like to thank Robert Little at Los Alamos National Laboratory for his help in the creation of the fission cross section file for MCNP.

References

1. Siewert, C. E., Benoist, P.; "Multigroup Transport Theory: I. Basic Analysis", *Nuclear Science and Engineering*, American Nuclear Society, **78**, 311-314 (1981).

2. Garcia, R. D. M., Siewert, C. E.; "Multigroup Transport Theory: II. Numerical Results", *Nuclear Science and Engineering*, American Nuclear Society, **78**, 315-323 (1981).

3. Siewert, C. E., Benoist, P.; "The F_N Method in Neutron-Transport Theory. Part I: Theory and Applications", *Nuclear Science and Engineering*, American Nuclear Society, **69**, 156-160 (1979).

4. Grandjean, P., Siewert, C. E.; "The F_N Method in Neutron-Transport Theory. Part II: Applications and Numerical Results", *Nuclear Science and Engineering*, American Nuclear Society, **69**, 161-168 (1979).

5. Garcia, R. D. M., Siewert, C. E.; "Multigroup Transport Theory with Anisotropic Scattering", *Journal of Computation Physics*, Academic Press, **46**, 237-270 (1982).

6. Garcia, R. D. M., Siewert, C. E.; "Multislab Multigroup Transport Theory with L^{th} Order Anisotropic Scattering", *Journal of Computation Physics*, Academic Press, **50**, 181-192 (1983).

7. Singleterry Jr., R. C.; *Neutron Transport Associated with the Galactic Cosmic Ray Cascade*; Doctoral Dissertation, University of Arizona; University Microfilms International; Ann Arbor, MI, USA; 1993.

8. Singleterry Jr., R. C.; *Computer Implementation of an Analytical Solution to the Neutral Particle Boltzmann Transport Equation for Heterogeneous Slabs*; Proceedings, International Conference on Mathematics and Computations, Reactor Physics, and Environmental Analysis; April 30 - May 4, 1995, Portland OR, USA; p.p. 1202-1213.

9. Briesmeister, J. F., ed.; *MCNP - A General Monte Carlo N-Particle Transport Code, Version 4A*; LA-12625-M, Los Alamos National Laboratory; November 1993.

10. Muskhelishvili, N. I. (translated from Russian by J. R. M. Radok); Singular Integral Equations, Second Edition, Dover Publications, Inc., New York, NY (1992).

11. Jahshan, S. N., Wemple, C. A., and Ganapol, B. D.; *Comparison of Analytical Transport and Stochastic Solutions for Neutron Slowing Down in an Infinite Medium*; Proceedings, Mathematical Methods and Supercomputing in Nuclear Applications; April 19-23, 1993; Karlsrude, Germany; p.p. 742-751.

12. Ganapol, B. D., Nigg, D. W., Jahshan, S. N., and Wemple, C. A.; *The Searchlight Problem for Neutrons in Semi-infinite Medium*; Proceedings, Mathematical Methods and Supercomputing in Nuclear Applications; April 19-23, 1993; Karlsrude, Germany; p.p. 137-147.

13. Bell, G. I., Glasstone, S.; Nuclear Reactor Theory, Robert E. Krieger Publishing Company, Malabar, FL (1970).

Table 1: Relative CPU Utilization

Source Type	c_i	Relative CPU Timings				
		F_N			MCNP	
		Time	N	Tol	Time	NPS
Beam	0.1	1.000	23	10^{-5}	32.713	1,000,000
	0.5	1.290	27	10^{-5}	48.757	1,000,000
	0.9	1.190	33	10^{-5}	113.277	1,000,000
	0.9, 0.5, 0.1	5.333	33	10^{-5}	88.067	1,000,000
	0.1, 0.5, 0.9	5.403	33	10^{-5}	35.037	1,000,000
Internal	0.1	1.141	21	10^{-5}	29.483	1,000,000
	0.5	1.782	37	10^{-5}	43.124	1,000,000
	0.9	1.505	29	10^{-5}	134.262	1,000,000
	0.9, 0.5, 0.1	5.740	33	10^{-5}	56.563	1,000,000
	0.1, 0.5, 0.9	5.844	33	10^{-5}	54.586	1,000,000
Critical	1.02	18.704	65	10^{-5}	354.122	599,150
	1.05	13.985	65	10^{-5}	179.323	597,631
	1.1	11.817	65	10^{-5}	104.243	599,423
	1.2	10.569	65	10^{-5}	65.686	599,466
	1.4	9.427	65	10^{-5}	49.313	599,717
	1.6	8.944	65	10^{-5}	43.227	599,974

Table 2: Criticality Parameters for the MCNP and F_N Models

c_i	Bell & Glasstone Table 2.6 Critical Widths (mfp)	F_N		MCNP			
		Critical Width (mfp)	Terms Used N	Averaged Combined k_{eff}	Standard Deviation	k_{eff} Interval	Confidence Level (%)
1.02	11.331	11.3310109	59	0.99951	0.00110	0.99730 - 1.00173	95
1.05	6.6004	6.6005275	59	0.85725	0.00100	0.85524 - 0.85926	95
1.1	4.2268	4.2266193	59	0.99930	0.00117	0.99694 - 1.00166	95
1.2	2.5786	2.5787586	59	1.00038	0.00111	0.99813 - 1.00262	95
1.4	1.4732	1.4732071	59	0.99866	0.00084	0.99698 - 1.00034	95
1.6	1.0240	1.0239260	59	1.00057	0.00085	0.99885 - 1.00229	95

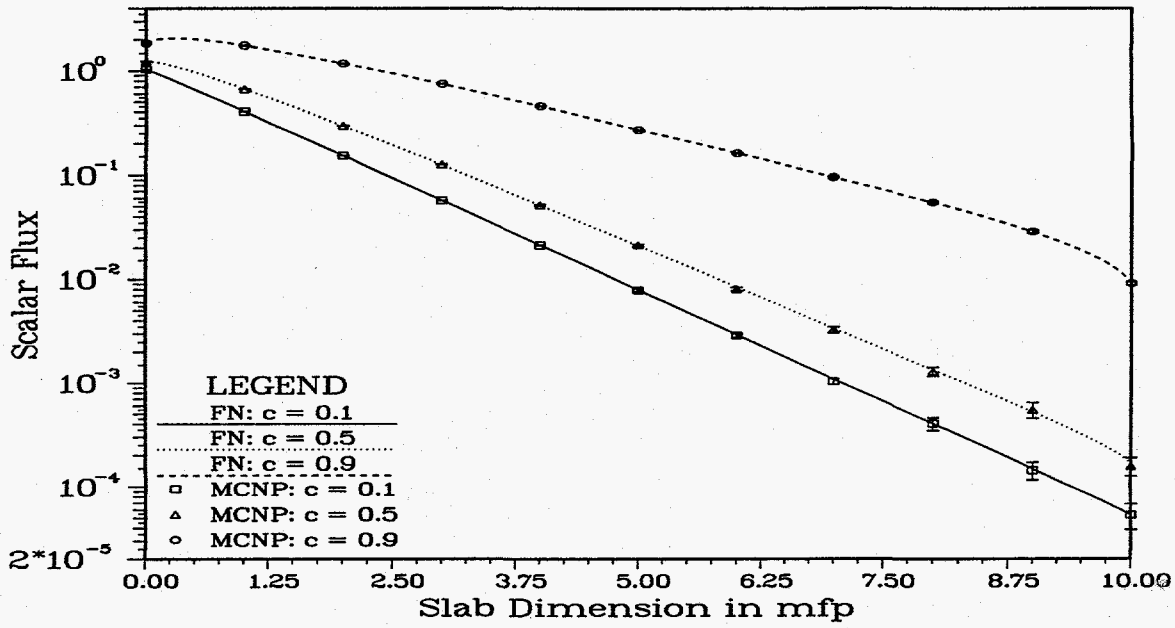

Figure 1: Scalar Flux for a Mono-directional Beam Source with Material c's Equal to 0.1, 0.5, and 0.9

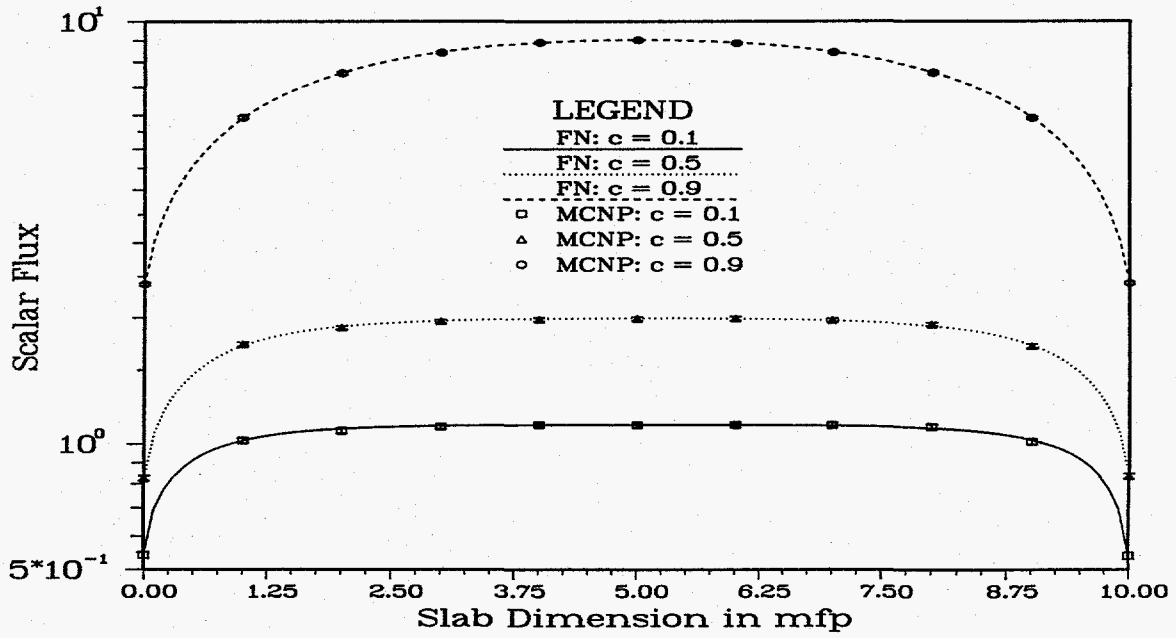

Figure 2: Scalar Flux for a Distributed Source with Material c's Equal to 0.1, 0.5, and 0.9

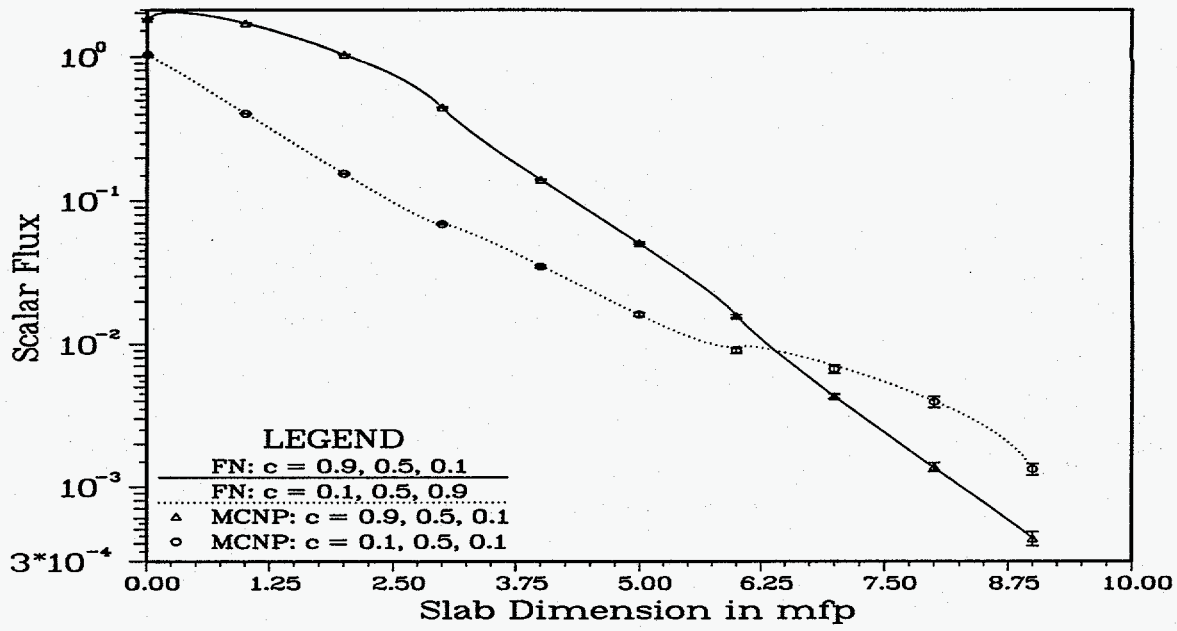

Figure 3: Scalar Flux for a Mono-directional Beam Source with Material c's Increasing and Decreasing

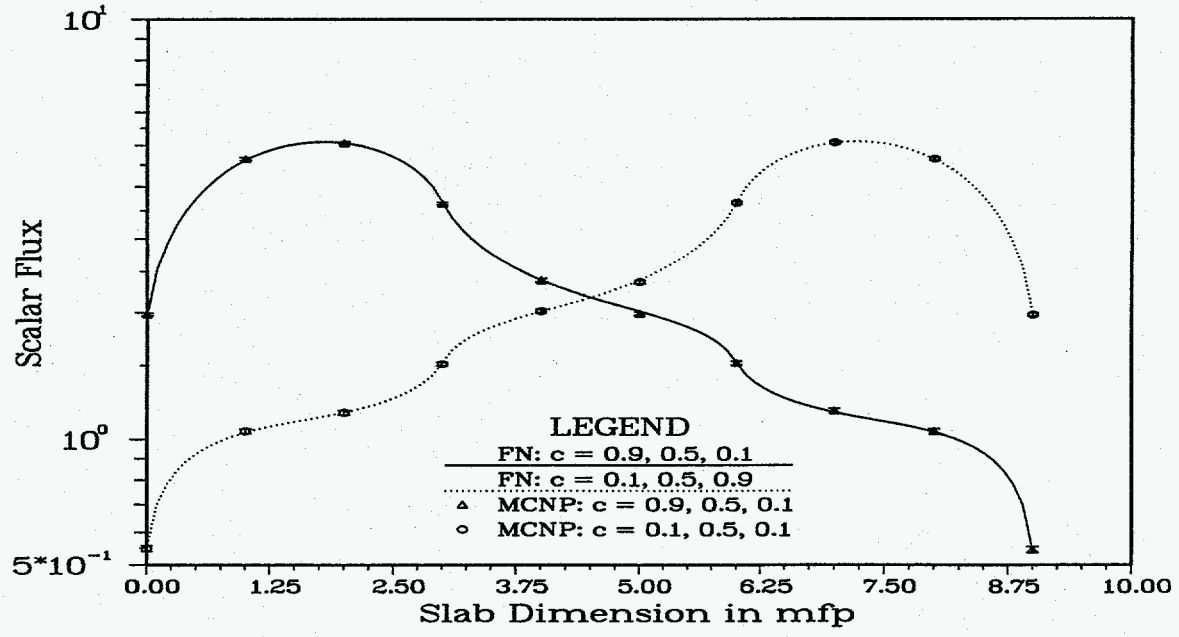

Figure 4: Scalar Flux for a Distributed Source with Material c's Increasing and Decreasing

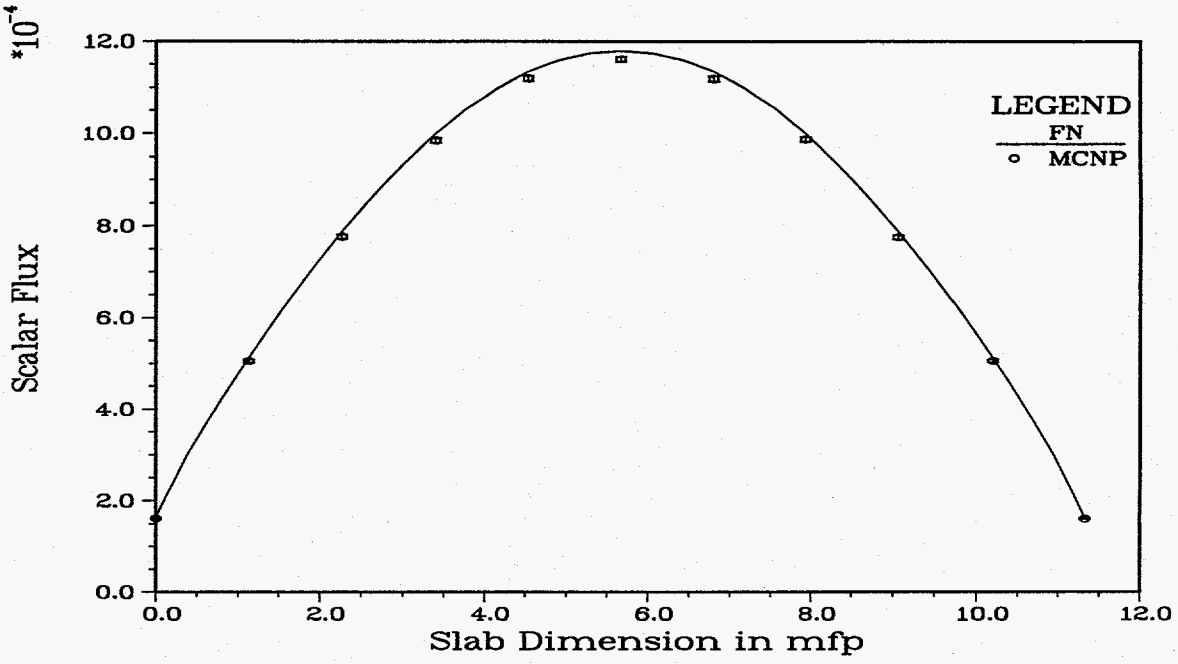

Figure 5: Scalar Flux for a Critical Slab with c=1.02

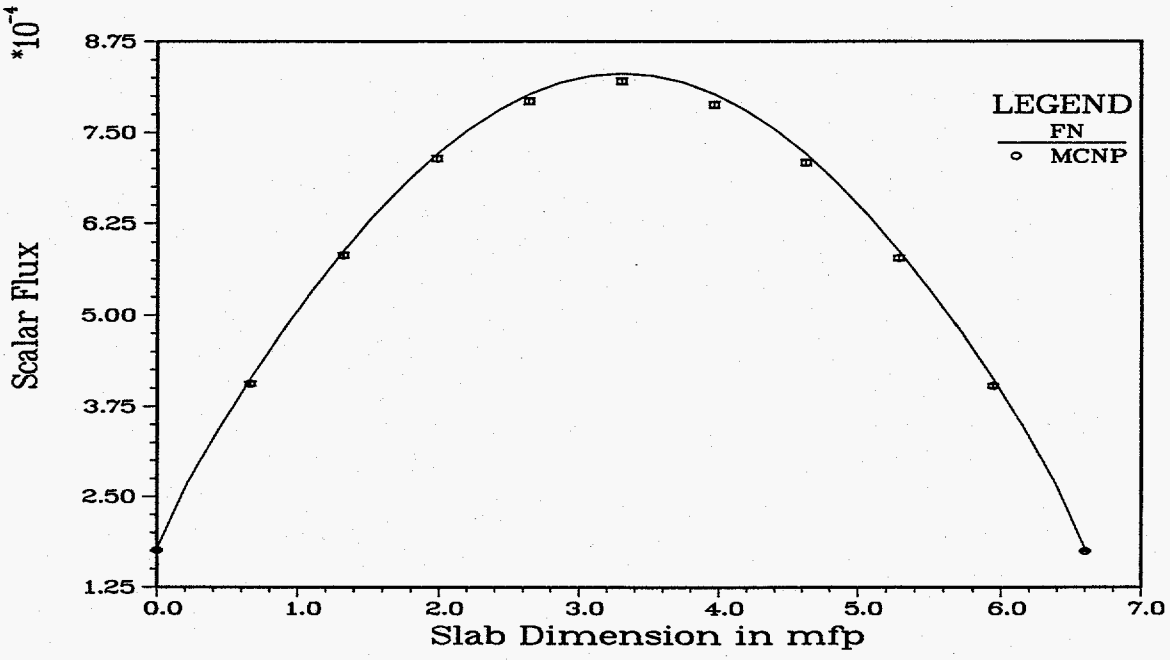

Figure 6: Scalar Flux for a Critical Slab with c=1.05

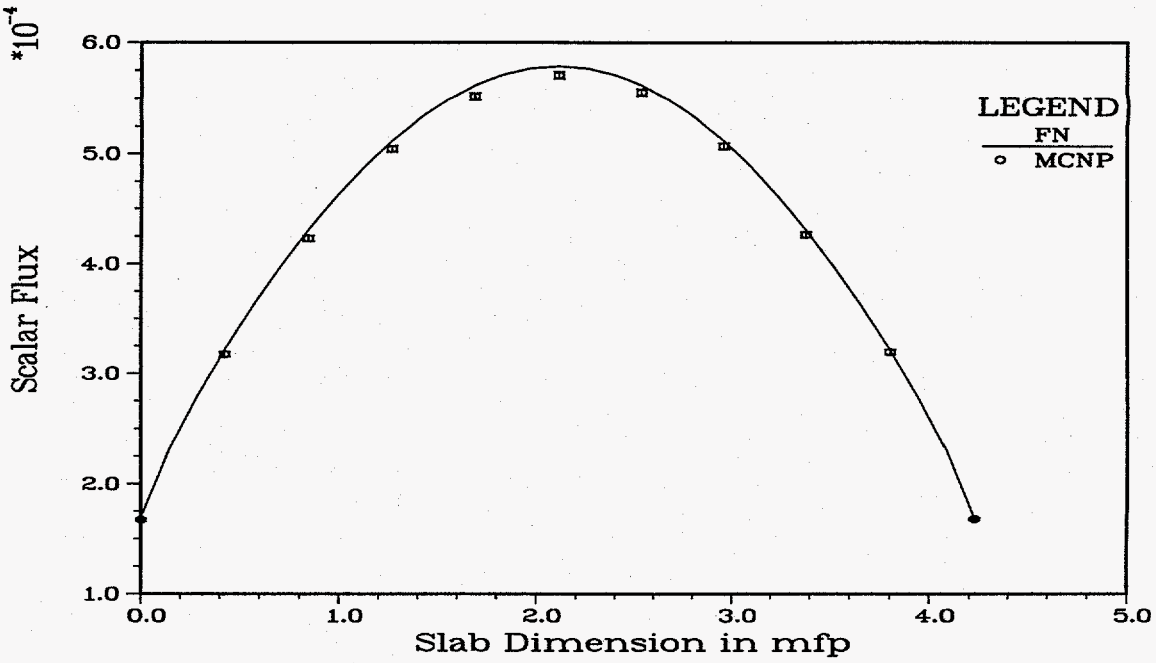

Figure 7: Scalar Flux for a Critical Slab with c=1.1

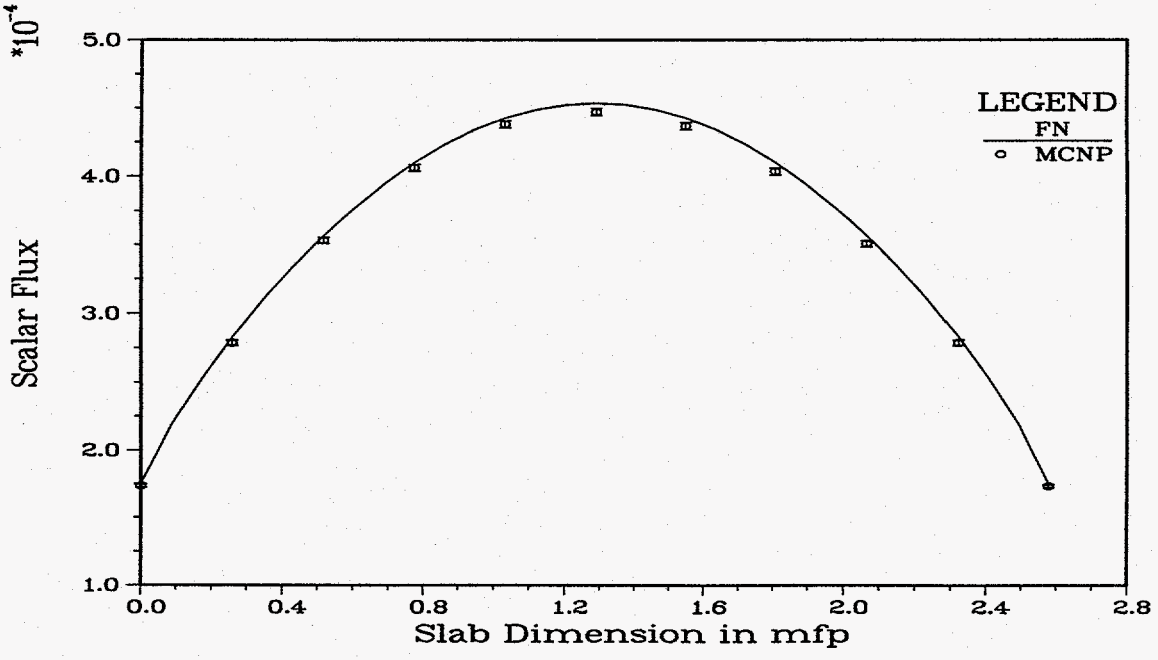

Figure 8: Scalar Flux for a Critical Slab with c=1.2

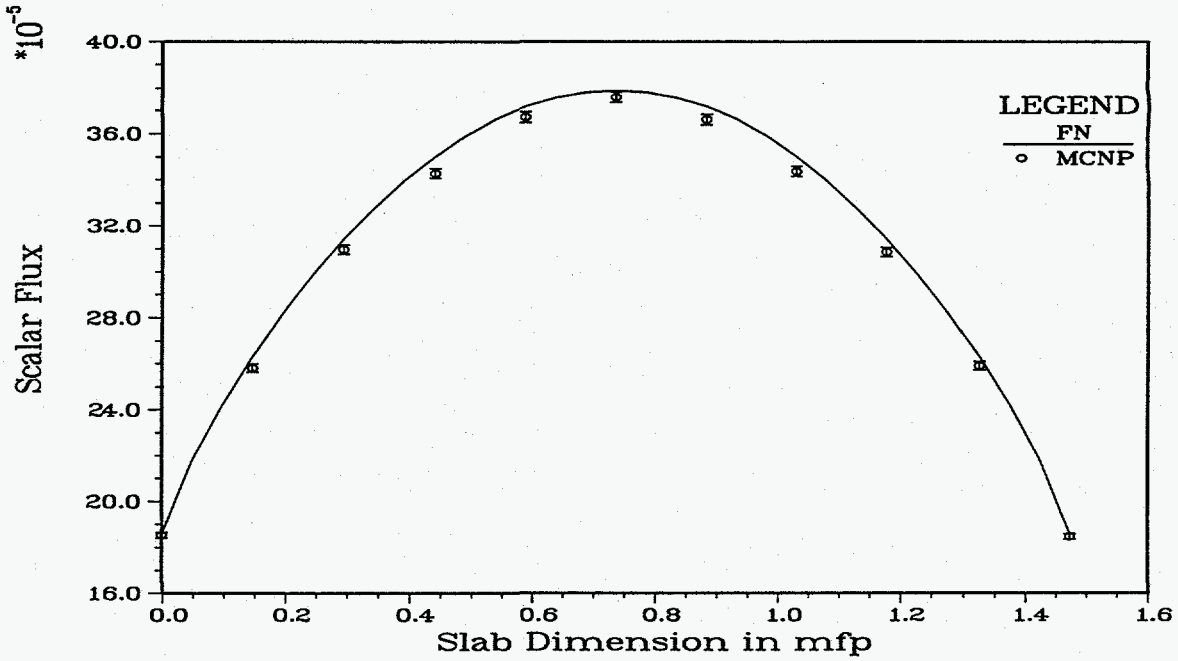

Figure 9: Scalar Flux for a Critical Slab with c=1.4

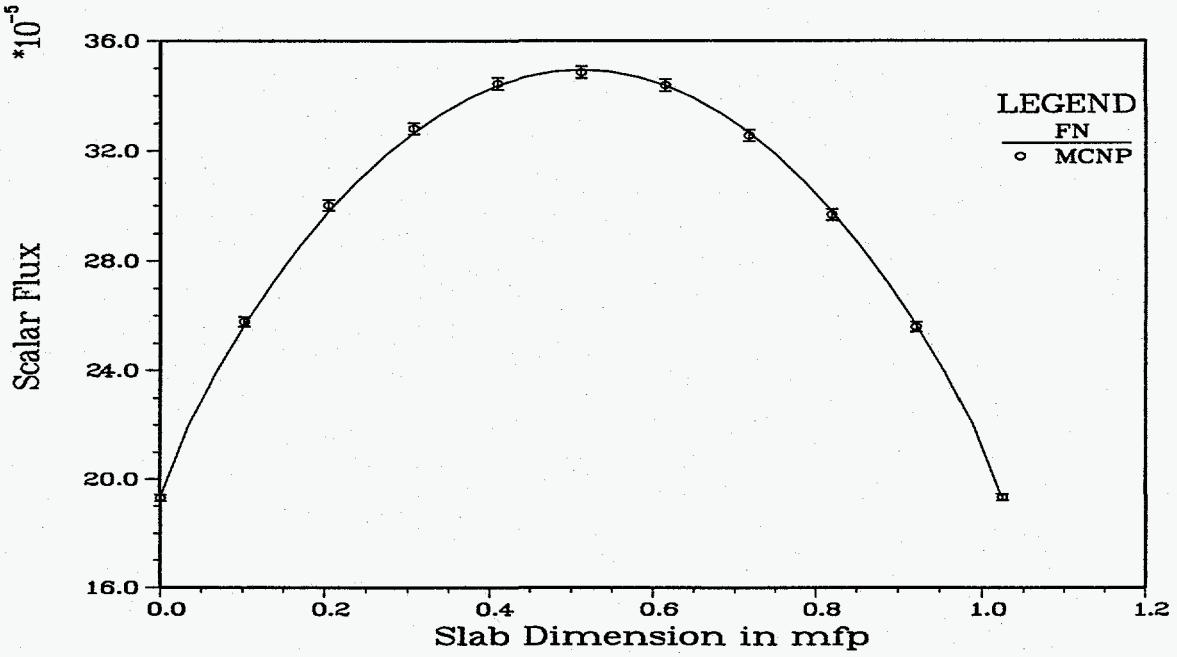

Figure 10: Scalar Flux for a Critical Slab with c=1.6

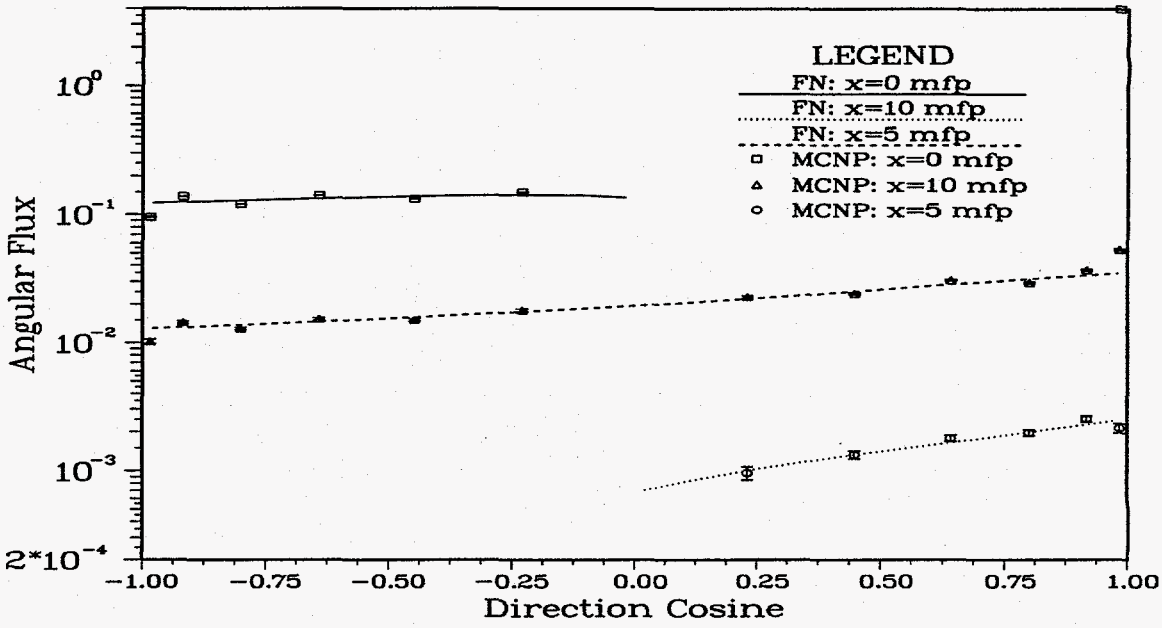

Figure 11: Angular Flux in the Slab for the Beam Source and a Material c of 0.9

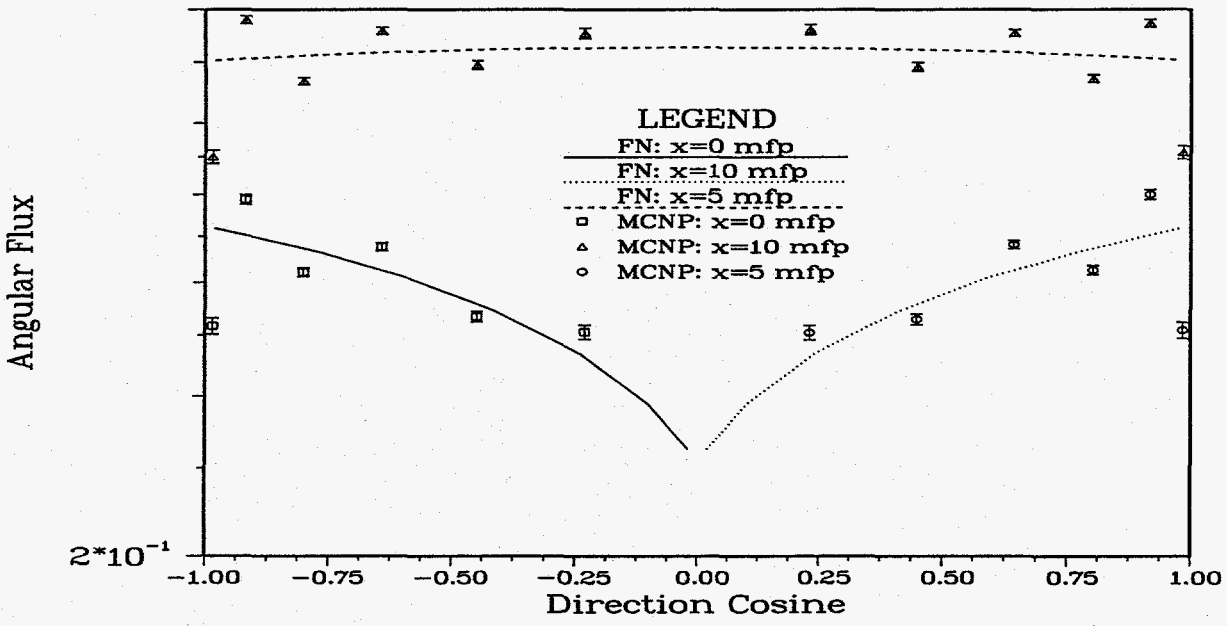

Figure 12: Angular Flux in the Slab for a Distributed Source and a Material c of 0.9

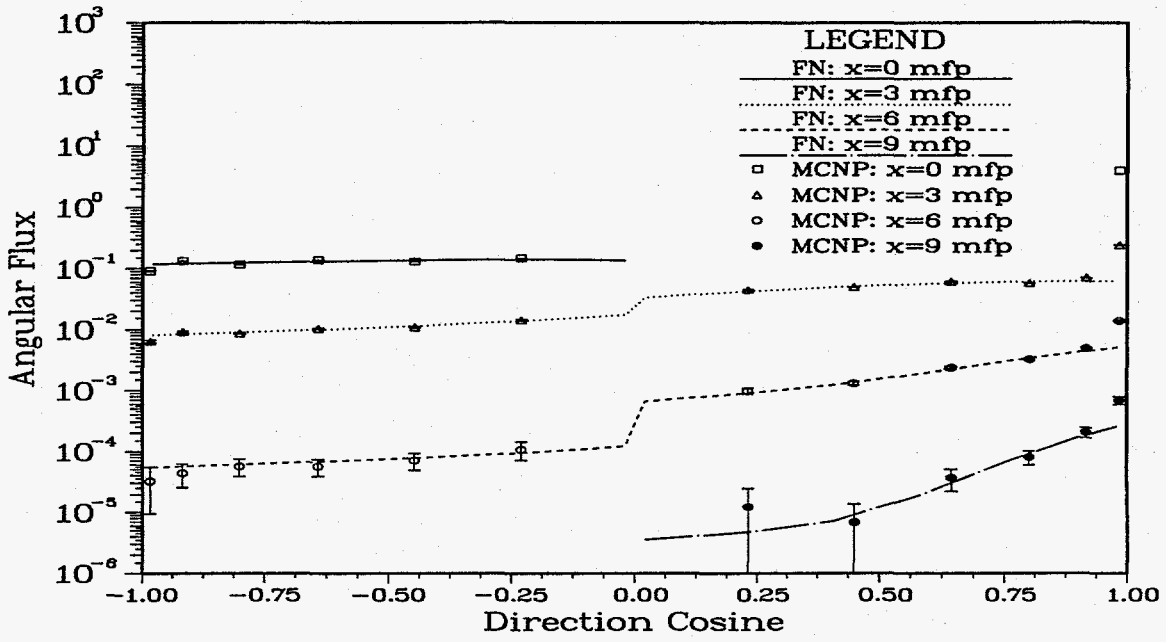

Figure 13: Angular Flux in the Slab for the Beam Source and Decreasing Material c's

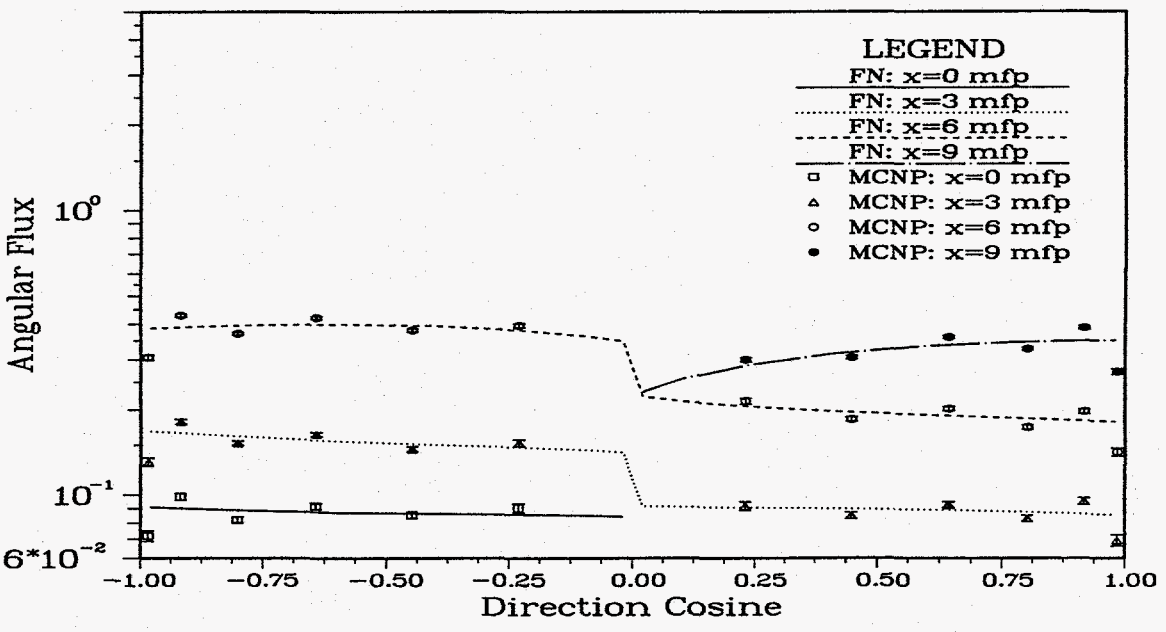

Figure 14: Angular Flux in the Slab for the Distributed Source and Increasing Material c's